Construction of a complete set of orthogonal Fourier-Mellin moment invariants for pattern recognition applications

Hui Zhang, Huazhong Shu, Pascal Haigron, Limin Luo, Baosheng Li

Construction of a complete set of orthogonal Fourier-Mellin moment invariants for pattern recognition applications

H. Zhang[1], H. Z. Shu[1, 5], P. Haigron[2, 3, 5], B.S. Li[4], L. M. Luo[1, 5]

[1]Laboratory of Image Science and Technology, School of Computer Science and Engineering, Southeast University, 210096 Nanjing, China

[2]INSERM, U642, 35042 Rennes, France

[3]Laboratoire Traitement du Signal et de l'Image, Université de Rennes I, 35042 Rennes, France

[4]Department of Radiation Oncology, Shandong Cancer Hospital, 250117 Jinan, China

[5]Centre de Recherche en Information Biomédicale Sino-français (CRIBs)

Information about the corresponding author

Huazhong Shu, Ph.D

Laboratory of Image Science and Technology

School of Computer Science and Engineering

Southeast University, 210096, Nanjing, China

Tel: 00-86-25-83 79 42 49

Fax: 00-86-25-83 79 26 98

Email: shu.list@seu.edu.cn

Abstract The completeness property of a set of invariant descriptors is of fundamental importance from the theoretical as well as the practical points of view. In this paper, we propose a general approach to construct a complete set of orthogonal Fourier-Mellin moment (OFMM) invariants. By establishing a relationship between the OFMMs of the original image and those of the image having the same shape but distinct orientation and scale, a complete set of scale and rotation invariants is derived. The efficiency and the robustness to noise of the method for recognition tasks are shown by comparing it with some existing methods on several data sets.

Key Words: Orthogonal Fourier-Mellin moments, Completeness, Similarity invariants, Moment invariants, Pattern recognition

1. Introduction

Description of objects invariant to geometric transformations such as translation, scale and rotation is a basic tool in pattern recognition. The performance of pattern recognition systems depends on the specific feature extraction technique used to represent a pattern. A popular class of invariant features is based on the moment techniques including geometric moment, complex moments and orthogonal moments [1-9]. Among them, moments with orthogonal basis functions can represent the image by a set of mutually independent descriptors and thus have a minimal amount of information redundancy. As noted by Ghorbel et al. [10, 11], the most important properties to assess by the image descriptors are: (1) invariance against some geometrical transformations (translation, rotation, scaling); (2) stability to noise, to blur, to non-rigid and small local deformations; and (3) completeness.

In the past decades, the construction of moment invariants and their application to pattern recognition have been extensively investigated [12-15]. Since the Zernike moments, pseudo-Zernike moments and orthogonal Fourier-Mellin moments (OFMMs) are all invariant under image rotation, they have been successfully used in the fields of image analysis and pattern recognition [16-24]. A comparative study of the Zernike moments and OFMMs in terms of recognition accuracy has been recently provided by Kan and Srinath [25]. It was shown that the OFMMs are better suited for character recognition tasks. The major drawback however, when using the orthogonal moments, is the lack of native scale invariance. To solve this problem, the normalization process [18] is often used to achieve the scale invariance. Such a process may lead to inaccuracy since the normalization of the images requires re-sampling and re-quantifying. In order to improve the accuracy, Chong et al. [26] recently proposed a method based on the properties of pseudo-Zernike polynomial to derive the scale invariants of pseudo-Zernike moments. A similar approach was then used to construct both translation and scale invariants of Legendre moments [27]. The problem of scale and translation invariants of Tchebichef moments has been investigated by Zhu et al. [28]. Discrete orthogonal moments such as Tchebichef moments yield better performance than the continuous orthogonal moments, but it is difficult to derive the rotation invariants. It was shown that the methods developed in [26-28] perform better than the classical approaches such as the image normalization method and indirect method. However, it seems difficult to obtain the completeness property by the above mentioned methods since no explicit formulation is derived for moment invariants.

A set of invariant descriptors is said to be complete if it satisfies the following property:

two objects have the same shape if and only if they have the same set of invariants [29]. A number of studies have been conducted on completeness. Flusser et al. proposed a complete set of rotation invariants by normalizing the complex moments [30, 31]. The construction of a complete set of similarity (translation, scale and rotation) invariant descriptors by means of some linear combinations of complex moments has been addressed by Ghorbel et al. [10].

In this paper, we propose a new method to construct a complete set of scale and rotation invariants extracted from OFMMs. We first establish a relationship between the OFMMs of the original image and those of the transformed image. Based on this relationship, the complete set of scale and rotation invariants can thus be achieved.

The organization of this paper is as follows. In Section 2, we review the definition of OFMMs and the approach proposed by Ghorbel et al. for constructing the complex moment invariants. Section 3 presents the way to derive a complete set of scale and rotation invariants of OFMMs. The experimental results for evaluating the performance of the proposed descriptors are provided in Section 4.

2. Orthogonal Fourier-Mellin moments

This section recalls the definition of OFMMs and briefly describes the method reported in Ref. [10].

2.1 Orthogonal Fourier-Mellin moments

The two-dimensional (2D) OFMM, Z_{pq}^{f}, of order p with repetition q of an image intensity function $f(r, \theta)$ is defined as [7]

$$Z_{pq}^{f} = \frac{p+1}{\pi} \int_{0}^{2\pi} \int_{0}^{1} Q_p(r) e^{-jq\theta} f(r,\theta) r dr d\theta, \qquad |q| \le p \tag{1}$$

where $Q_p(r)$ is a set of radial polynomials given by

$$Q_p(r) = \sum_{k=0}^{p} c_{p,k} r^k \,, \tag{2}$$

with

$$c_{p,k} = (-1)^{p+k} \frac{(p+k+1)!}{(p-k)!k!(k+1)!} \,. \tag{3}$$

Since OFMMs are defined in terms of polar coordinates (r, θ) with $|r| \le 1$, the computation of OFMMS requires a linear transformation of the image coordinates to a suitable domain inside a unit circle. Here we use the mapping transformation proposed by Chong et al. [26], which is shown in Fig. 1. Based on this transformation, we have the following discrete approximation of equation (1):

$$Z_{pq}^{f} = \frac{p+1}{\pi} \sum_{i=0}^{N-1} \sum_{j=0}^{N-1} Q_p(r_{ij}) e^{-jq\theta_{ij}} f(i,j) \,, \tag{4}$$

where the image coordinate transformation to the interior of the unit circle is given by

$$r_{ij} = \sqrt{(c_1 i + c_2)^2 + (c_1 j + c_2)^2} \,, \quad \theta_{ij} = \tan^{-1}\left(\frac{c_1 j + c_2}{c_1 i + c_2} \right) \tag{5}$$

with $c_1 = \dfrac{\sqrt{2}}{N-1}$ $\quad c_2 = \dfrac{1}{\sqrt{2}}$.

2.2 A complete set of invariants extracted from complex moments

Ghorbel et al. proposed a complete set of scale and rotation invariants of complex moments given by [10]

$$J_f(p,q) = \Gamma_f^{-(p+q+2)} e^{-i(p-q)\theta_f} c_f(p,q) \tag{6}$$

where $\theta_f = \arg(c_f(1,0))$, $\Gamma_f = \sqrt{c_f(0,0)}$, and $c_f(p,q)$ is the complex moment of an image function $f(x, y)$ defined as

$$\begin{aligned} c_f(p,q) &= \int_{-\infty}^{\infty} \int_{-\infty}^{\infty} (x+iy)^p (x-iy)^q f(x,y) dxdy \\ &= \int_0^{\infty} \int_0^{2\pi} r^{p+q+1} e^{i(p-q)\theta} f(r,\theta) dr d\theta \end{aligned} \qquad p,\ q \ge 0. \tag{7}$$

It can be easily verified that the set of invariants is complete since

$$c_f(p,q) = \Gamma_f^{(p+q+2)} e^{i(p-q)\theta_f} J_f(p,q) . \tag{8}$$

Note that in [10], the translation invariance was achieved by transforming the origin of the image to the geometric center before the calculation of the moments.

3. Method

In this section, a general approach is described to derive a complete set of OFMM invariants. We use here the same method to achieve the translation invariance as described in [10]. That is, the origin of the coordinate system is taken at the center of mass of the object to achieve the translation invariance. This center of mass, (x_c, y_c), can be computed from the first geometric moments of the object as follows.

$$x_c = \frac{m_{10}}{m_{00}}, \quad y_c = \frac{m_{01}}{m_{00}}, \tag{9}$$

where m_{pq} are the $(p+q)$th order geometric moments defined by

$$m_{pq} = \int_{-\infty}^{\infty}\int_{-\infty}^{\infty} x^p y^q f(x,y)dxdy . \tag{10}$$

Let $U_m(r) = (Q_0(r), Q_1(r), \cdots, Q_m(r))^T$ and $M_m(r) = (r^0, r^1, \cdots, r^m)^T$ be two vectors, where the superscript T indicates the transposition, we have

$$U_m(r) = C_m M_m(r) , \tag{11}$$

where $C_m = (c_{i,j})$, with $0 \le j \le i \le m$, is a $(m+1)\times(m+1)$ lower triangular matrix whose element $c_{i,j}$ is given by Eq. (3).

Since all the diagonal elements of C_m, $c_{l,l} = \dfrac{(2l+1)!}{l!(l+1)!}$, are not zero, the matrix C_m is non-singular, thus

$$M_m(r) = (C_m)^{-1} U_m(r) = D_m U_m(r) , \tag{12}$$

where $D_m = (d_{i,j})$, with $0 \le j \le i \le m$, is the inverse matrix of C_m. It is also a $(m+1)\times(m+1)$ lower triangular matrix. The computation of the elements of D_m is given in the following Proposition.

Proposition 1. For the lower triangular matrix C_m whose elements $c_{i,j}$ are defined by Eq. (3), the elements of the inverse matrix D_m are given as follows

$$d_{i,j} = \frac{(2j+2)i!(i+1)!}{(i-j)!(i+j+2)!}. \tag{13}$$

The proof of Proposition 1 is given in Appendix.

Let f and g be two images display the same pattern but with distinct orientation (β) and scale (λ), i.e., $g(r, \theta) = f(r/\lambda, \theta-\beta)$. The OFMM of the image intensity function $g(r, \theta)$ is defined as

$$\begin{aligned} Z_{pq}^{g} &= \frac{p+1}{\pi}\int_0^{2\pi}\int_0^1 Q_p(r)e^{-jq\theta}g(r,\theta)rdrd\theta \\ &= \lambda^2 e^{-jq\beta}\frac{p+1}{\pi}\int_0^{2\pi}\int_0^1 Q_p(\lambda r)e^{-jq\theta}f(r,\theta)rdrd\theta, \end{aligned} \tag{14}$$

Letting $U_m(\lambda r) = (Q_0(\lambda r), Q_1(\lambda r), \cdots, Q_m(\lambda r))^T$ and $M_m(\lambda r) = (1, (\lambda r)^1, \cdots, (\lambda r)^m)^T$, it can be seen from Eq. (11) that

$$U_m(\lambda r) = C_m M_m(\lambda r). \tag{15}$$

On the other hand,

$$\begin{aligned} M_m(\lambda r) &= diag(1, \lambda^1, \cdots, \lambda^m)(1, r^1, \cdots, r^m)^T \\ &= diag(1, \lambda^1, \cdots, \lambda^m)M_m(r). \end{aligned} \tag{16}$$

Substituting Eqs. (16) and (12) into Eq. (15), we obtain

$$U_m(\lambda r) = C_m diag(1, \lambda^1, \cdots, \lambda^m)D_m U_m(r). \tag{17}$$

By expanding Eq. (17), we have

$$Q_p(\lambda r) = \sum_{k=0}^{p} Q_k(r) \sum_{l=k}^{p} \lambda^l c_{p,l} d_{l,k} \,. \tag{18}$$

With the help of Eq. (18), Eq. (14) can be rewritten as

$$\begin{aligned} Z_{pq}^{g} &= \lambda^2 e^{-jq\beta} \frac{p+1}{\pi} \int_0^{2\pi} \int_0^1 Q_p(\lambda r) e^{-jq\theta} f(r,\theta) r dr d\theta \\ &= \lambda^2 e^{-jq\beta} \frac{p+1}{\pi} \int_0^{2\pi} \int_0^1 \left(\sum_{k=0}^{p} Q_k(r) \sum_{l=k}^{p} \lambda^l c_{p,l} d_{l,k} \right) e^{-jq\theta} f(r,\theta) r dr d\theta \\ &= e^{-jq\beta} \sum_{k=0}^{p} \frac{p+1}{k+1} \times \frac{k+1}{\pi} \sum_{l=k}^{p} \lambda^{l+2} c_{p,l} d_{l,k} \int_0^{2\pi} \int_0^1 Q_k(r) e^{-jq\theta} f(r,\theta) r dr d\theta \\ &= e^{-jq\beta} \sum_{k=0}^{p} \frac{p+1}{k+1} \left(\sum_{l=k}^{p} \lambda^{l+2} c_{p,l} d_{l,k} \right) Z_{kq}^{f}. \end{aligned} \tag{19}$$

The above equation shows that the 2D scaled and rotated OFMMs, Z_{pq}^{g}, can be expressed as a linear combination of the original OFMMs Z_{kq}^{f} with $0 \le k \le p$. Based on this relationship, we can construct a complete set of both rotation and scale invariants I_{pq}^{f} which is described in the following theorem.

Theorem 1. For a given integer q and any positive integer p, let

$$I_{pq}^{f} = \sum_{k=0}^{p} e^{-jq\theta_f} \frac{p+1}{k+1} \left(\sum_{l=k}^{p} \Gamma_f^{-(l+2)} c_{p,l} d_{l,k} \right) Z_{kq}^{f} \,, \tag{20}$$

with $\theta_f = \arg(Z_{11}^{f})$ and $\Gamma_f = \sqrt{Z_{00}^{f}}$. Then, I_{pq}^{f} is invariant to both image rotation and scaling.

The proof of Theorem 1 is given in Appendix.

Eq. (20) can be expressed in matrix form as

$$\begin{pmatrix} I_{0q}^{f} \\ I_{1q}^{f} \\ \vdots \\ I_{pq}^{f} \end{pmatrix} = e^{-jq\theta_f} diag\left(1,2,\cdots,p+1\right) C_p diag\left(\Gamma_f^{-2},\Gamma_f^{-3},\cdots,\Gamma_f^{-(p+2)}\right) D_p diag\left(1,\frac{1}{2},\cdots,\frac{1}{p+1}\right) \begin{pmatrix} Z_{0q}^{f} \\ Z_{1q}^{f} \\ \vdots \\ Z_{pq}^{f} \end{pmatrix}. \tag{21}$$

It is easy to verify that the set of invariants is complete by rewriting Eq. (21) as

$$\begin{pmatrix} Z_{0q}^{f} \\ Z_{1q}^{f} \\ \vdots \\ Z_{pq}^{f} \end{pmatrix} = e^{jq\theta_f}\, diag(1,2,\cdots,p+1)\, C_p\, diag\left(\Gamma_f{}^{2},\Gamma_f{}^{3},\cdots,\Gamma_f{}^{(p+2)}\right) D_p\, diag\left(1,\frac{1}{2},\cdots,\frac{1}{p+1}\right) \begin{pmatrix} I_{0q}^{f} \\ I_{1q}^{f} \\ \vdots \\ I_{pq}^{f} \end{pmatrix}. \quad (22)$$

Thus, we have

$$Z_{pq}^{f} = \sum_{k=0}^{p} e^{jq\theta_f}\, \frac{p+1}{k+1} \left(\sum_{l=k}^{p} \Gamma_f{}^{(l+2)} c_{p,l} d_{l,k} \right) I_{kq}^{f} \quad (23)$$

The above equation shows that the set of invariants is complete.

4. Experimental results

This section is intended to test the performance of the complete family of similarity invariants introduced in this paper using a set of gray-level images.

In the first experiment, a toy cat image whose size is 128×128 pixels is chosen from the well-known Columbia database [32] (Fig. 2). The proposed invariant descriptors are compared to the complete set of complex moment invariants (CMI) reported in [10]. To make the comparison possible between all families of invariants, we rearrange the complex moment invariants following the scheme presented in Ref. [10] through the path (1, 0)→1, (0, 1)→2, (2, 0)→3, (1, 1)→4, (0, 2)→5, (3, 0)→6, and so on. Let M be the maximum order of complex moment invariant, and let $C_C^f(M) = (J_f(1,0), J_f(0,1), \ldots, J_f(M,0), \ldots, J_f(0,M))$, where $J_f(p, q)$ are defined by Eq. (6). The dimension of $C_C^f(M)$ is $(M+1)(M+2)/2-1$. For comparison purpose, we also define the vector $C_{FM}^f(M) = (I_f(1,0), I_f(1,1), \ldots, I_f(M,0), \ldots, I_f(M,M))$ for OFMM invariants (OFMMI). The dimension of $C_{FM}^f(M)$ is also $(M+1)(M+2)/2-1$. In this experiment $M = 4$ is chosen, that is, 14 invariants from first to fourth order are used.

We define the relative error between the two sets of moment invariants corresponding to

the original image $f(x, y)$ and the transformed image $g(x, y)$ as

$$E_M(f,g) = \frac{\| C^f(M) - C^g(M) \|}{\| C^f(M) \|}, \tag{24}$$

where ||.|| is the Euclidean norm.

To test the invariance against rotation, we have rotated the original image from 0° to 180° with interval 5°. Because the magnitude of the OFMM is invariant to image rotation, we also take it as rotation invariant feature of the underlying image function. Fig. 3 compares the relative errors between the proposed method, CMI and the magnitude of the OFMMs (MOFMM) using Eq. (24). It can be seen from this figure that the OFMMI outperforms the other two methods, whatever the rotational angle. We then evaluate the invariance of the proposed descriptors with regard to image scaling. The toy cat image is scaled by a factor varying from 0.1 to 2 with interval 0.05. Fig. 4 shows the relative errors of the OFMMI, CMI, the normalization method presented in [18] and the scale invariants of OFMM derived by the method presented in Ref. [26] (we call it Chong's method for abbreviation). Plots show that, in most cases, the relative errors of OFMMI and Chong's method are lower than those of the CMI and normalization method. To test the robustness to noise, we have respectively added a white Gaussian noise (with mean $\mu = 0$ and different variances) and the salt-and-pepper noise (with different noise densities). Results are respectively depicted in Fig. 5 and Fig. 6. It can be seen that, if the relative error increases with the noise level, the proposed descriptors are more robust to noise than the CMI and Chong's method.

We also compare the computational speed of the OFMMI with that of the CMI and other methods. The computation time required in the above experiments for different methods is listed in Table 1 where the moment invariants of order up to $M = 4$ are calculated. Note that

the program was implemented in MATLAB 6.5 on a PC P4 2.4 GHZ, 512M RAM, and the computation of the OFMMIs was performed from Eq. (21). It can be seen that the OFMMI is faster than most of the other methods, this is due to the following two facts: (1) the fast algorithm presented in Ref. [23] was applied; (2) the matrix representation is very useful and efficient for software packages such as MATLAB.

We now test the classification accuracy of the proposed method, CMI and Chong's method with scaled and rotated image in both noise-free and noisy conditions. For the recognition task, we use the following feature vector

$$V = [I_1, I_2, I_3, I_4, I_5, I_6, I_7], \tag{25}$$

where $I_j, j = 1, 2, \ldots, 7$, denote the second and third order of CMI or OFMM invariants. The objective of a classifier is to identify the class of the unknown input object. During the classification, features of the unknown object are compared to a set of testing samples. The Euclidean distance is used as the classification measure and is defined by

$$d(V_s, V_t^{(k)}) = \sum_{j=1}^{7} (I_j^s - I_j^t)^2 , \tag{26}$$

where V_s is the *7*-dimensional feature vector of unknown sample, and $V_t^{(k)}$ is the testing vector of class *k*. The classification accuracy is defined as

$$\eta = \frac{Number\ of\ correctly\ classified\ images}{The\ total\ number\ of\ images\ used\ in\ the\ test} \times 100\% . \tag{27}$$

Fig. 7 shows a set of object images selected from the Coil-100 image database of Columbia University [32]. The reason for choosing such a set is that the objects (three toy cars, three blocks, ANACIN and TYLENOL packs) can be easily misclassified due to their similarity. This set is then transformed by scaling and rotating the original set with scale

factor $\lambda \in \{0.5, 0.75, 1, 1.5, 2\}$ and rotation angle $\beta \in \{30°, 60°, \ldots\ldots, 330°, 360°\}$, forming a set of 480 images. This is followed by adding the salt-and-pepper noise with different noise densities. The feature vector based on our method is used to classify these images and its recognition accuracy is compared to CMI as well as Chong's method. Table 2 shows the classification results using the full set of features. One can observe from this table that the high recognition rates are obtained in noise-free case. The recognition accuracy decreases with increasing noise level. However, the proposed method performs better than the CMI and Chong's method in terms of the recognition accuracy for noisy images.

In the last experiment, a set of alphanumeric characters whose size are 50×50 pixels shown in Fig. 8 is used for recognition task. The images are transformed by scaling and rotating the original set with scale factor $\lambda \in \{0.5, 1, 2\}$ and rotation angle $\beta \in \{15°, 30°, \ldots\ldots, 345°, 360°\}$, forming a set of 576 images. The salt-and-pepper noise with different noise densities has been added. Some examples of the test images are illustrated in Fig. 9. The classification results are listed in Table 3. It can be seen that our method is more robust than other methods for noisy images.

5. Conclusion

In this paper, we have presented a novel method to derive a complete set of OFMM invariants. Since the proposed method extracts the invariant feature from the orthogonal Fourier-Mellin moments of the original image, no image normalization process is required. Experimental results show that our method has a better classification accuracy and is more robust to noise when compared to the existing moment-based methods.

Acknowledgement: This work was supported by Program for Changjiang Scholars and Innovative Research Team in University and by the National Natural Science Foundation of China under Grant 30670617.

References

1. M.K. Hu, Visual pattern recognition by moment invariants, IRE Transactions on Information Theory, 8 (1962) 179-187.
2. J. Flusser, T. Suk, Pattern recognition by affine moment invariants, Pattern Recognition, 26 (1993) 167-174.
3. M. Teague, Image analysis via the general theory of moments, Journal Optical Society America, 70 (1980) 920-930.
4. C.H. Teh, R.T. Chin, On image analysis by the method of moments, IEEE Transactions on Pattern Analysis and Machine Intelligence, 10 (1988) 496-513.
5. S.S. Reddi, Radial and angular moment invariants for image identification, IEEE Transactions on Pattern Analysis and Machine Intelligence, 3 (1981) 240-242.
6. Y.S. Abu-Mostafa, D. Psaltis, Recognitive aspects of moment invariants, IEEE Transactions on Pattern Analysis and Machine Intelligence, 6 (1984) 698-706.
7. Y.L. Sheng, L.X.Shen, Orthogonal Fourier-Mellin moments for invariant pattern recognition. Journal Optical Society America, 11 (1994) 1748-1757.
8. T. Xia, H.Q. Zhu, H.Z. Shu, P. Haigron, L.M. Luo, Image description with generalized pseudo-Zernike moments, Journal Optical Society America, 24 (2007) 50-59.
9. S. Rodtook, S.S. Makhanov, Numerical experiments on the accuracy of rotation moments invariants, Image and Vision Computing, 23 (2005) 577-586.
10. F. Ghorbel, S. Derrode, R. Mezhoud, T. Bannour, S. Dhahbi, Image reconstruction from a complete set of similarity invariants extracted from complex moments, Pattern

Recognition Letters, 27 (2006) 1361-1369.

11. S. Derrode, F. Ghorbel, Robust and efficient Fourier-Mellin transform approximations for invariant grey-level image description and reconstruction, Computer Vision and Image Understanding, 83 (2001) 57-78.
12. Y. Li, Reforming the theory of invariant moments for pattern recognition, Pattern Recognition, 25 (1992) 723-730.
13. J. Liu, T.X. Zhang, Fast algorithm for generation of moment invariants, Pattern Recognition, 37 (2004) 1745-1756.
14. D. Xu, H. Li, Geometric moment invariants, Pattern Recognition, 41 (2008) 240-249.
15. Y. C. Chim, A. A. Kassim, Y. Ibrahim, Character recognition using statistical moments, Image and Vision Computing, 17 (1999) 299-307.
16. Z.J. Miao, Zernike moment-based image shape analysis and its application, Pattern Recognition Letters, 21 (2000) 169-177.
17. W.Y. Kim and Y.S. Kim, A region-based shape descriptor using Zernike moments, Signal Processing: Image Communication, 16 (2000) 95-102.
18. A. Kontanzard, Y.H. Hong, Invariant image recognition by Zernike moments, IEEE Transactions on Pattern Analysis and Machine Intelligence, 12 (1990) 489-497.
19. R.R. Bailey and M.D. Srinath, Orthogonal moment features for use with parametric and non-parametric classifiers, IEEE Transactions on Pattern Analysis and Machine Intelligence, 18 (1996) 389-399.
20. A. Broumandnia, J. Shanbehzadeh, Fast Zernike wavelet moments for Farsi character recognition, Image and Vision Computing, 25 (2007) 717-726.

21. T.J. Bin, A. Lei, J.W. Cui, W.J. Kang, D.D. Liu, Subpixel edge location based on orthogonal Fourier–Mellin moments, Image and Vision Computing, 26 (2008) 563-569.

22. B. Ye, Improvement of orthogonal Fourier-Mellin moments, Proceedings of SPIE - The International Society for Optical Engineering 5985 PART II, (2005) 598531.

23. G.A. Papakostas, Y.S. Boutalis, D.A. Karras, B.G. Mertzios, Fast numerically stable computation of orthogonal Fourier-Mellin moments, IET Computer Vision 1 (2007) 11-16.

24. B. Fu, J.Z. Zhou, J.Q. Wen, An efficient algorithm for fast computation of orthogonal Fourier-Mellin moments, Proceedings of SPIE - The International Society for Optical Engineering 5985 PART II, (2005) 59853A.

25. C. Kan, M.D. Srinath, Invariant character recognition with Zernike and orthogonal Fourier-Mellin moments, Pattern Recognition, 35 (2002) 143-154.

26. C.W. Chong, P. Raveendran, R. Mukundan, The scale invariants of pseudo-Zernike moments, Pattern Analysis and Applications 6 (2003) 176-184.

27. C.W. Chong, P. Raveendran, R. Mukundan, Translation and scale invariants of Legendre moments, Pattern Recognition, 37 (2004) 119-129.

28. H.Q. Zhu, H.Z. Shu, T. Xia, L.M. Luo, J.L. Coatrieux, Translation and scale invariants of Tchebichef moments, Pattern Recognition, 40 (2007) 2530-2542.

29. T.R. Crimmins, A complete set of Fourier descriptors for two dimensional shape, IEEE Transactions on Systems, Man and Cybernetics, 121 (1982) 848– 855.

30. J. Flusser, On the independence of rotation moment invariants. Pattern Recognition, 33 (2000) 1405–1410.

31. J. Flusser, On the inverse problem of rotation moment invariants. Pattern Recognition, 35 (2002) 3015–3017.

32. http://www1.cs.columbia.edu/CAVE/software/softlib/coil-20.php

33. M. Petkovsek, H. S. Wilf, and D. Zeilberger, A=B, AK Peters (1996). (available on line at the University of Pennsylvania).

Appendix

Proof of Proposition 1. To prove the proposition, we need to demonstrate the following relation

$$\sum_{s=l}^{k} c_{k,s} d_{s,l} = \delta_{k,l} . \tag{A1}$$

For $k = l$, we have

$$c_{k,k} d_{k,k} = \frac{(2k+1)!}{k!(k+1)!} \times \frac{(2k+2)k!(k+1)!}{(2k+2)!} = 1 . \tag{A2}$$

For $l < k$, we have

$$\begin{aligned} \sum_{s=l}^{k} c_{k,s} d_{s,l} &= \sum_{s=l}^{k} (-1)^{k+s} \frac{(k+1+s)!(2l+2)}{(k-s)!(s-l)!(s+l+2)!} \\ &= (-1)^{k} (2l+2) \sum_{s=l}^{k} F(k,l,s), \end{aligned} \tag{A3}$$

where

$$F(k,l,s) = \frac{(-1)^{s} (k+1+s)!}{(k-s)!(s-l)!(s+l+2)!} . \tag{A4}$$

Letting

$$G(k,l,s) = \frac{(-1)^{s+1} (k+1+s)!}{(k+1-s)!(s-l)!(s+l+1)!} \frac{(k+1-s)(s-l)}{(k-l)(k+l+2)}, \tag{A5}$$

it can then be easily verified that

$$F(k,l,s) = G(k,l,s+1) - G(k,l,s) . \tag{A6}$$

Thus

$$\begin{aligned} \sum_{s=l}^{k} F(k,l,s) &= \sum_{s=l}^{k} [G(k,l,s+1) - G(k,l,s)] \\ &= G(k,l,k+1) - G(k,l,l) = 0, \end{aligned} \tag{A7}$$

we deduce from Eq. (A3) that

$$\sum_{s=l}^{k} c_{k,s} d_{s,l} = 0 \quad \text{for } l < k.$$

The proof is now complete.

Note that the proof of Proposition 1 was inspired by a technique proposed by Petkovsek et al [33].

Proof of Theorem 1. Eq. (20) can be rewritten in matrix form as

$$\begin{pmatrix} I_{0q}^{g} \\ I_{1q}^{g} \\ \vdots \\ I_{pq}^{g} \end{pmatrix} = e^{-jq\theta_g} diag(1,2,\cdots,p+1) C_p \times diag(Z_{00}^{g\,-2/2}, Z_{00}^{g\,-3/2}, \cdots, Z_{00}^{g\,-(p+2)/2}) D_p diag(1, \frac{1}{2}, \cdots, \frac{1}{p+1}) \begin{pmatrix} Z_{0q}^{g} \\ Z_{1q}^{g} \\ \vdots \\ Z_{pq}^{g} \end{pmatrix} \tag{A8}$$

Using the same representation, Eq. (19) can be expressed by

$$\begin{pmatrix} Z_{0q}^{g} \\ Z_{1q}^{g} \\ \vdots \\ Z_{pq}^{g} \end{pmatrix} = e^{-jq\beta} diag(1,2,\cdots,p+1) C_p diag(\lambda^2, \lambda^3, \cdots, \lambda^{p+2}) D_p \times diag(1, \frac{1}{2}, \cdots, \frac{1}{p+1}) \begin{pmatrix} Z_{0q}^{f} \\ Z_{1q}^{f} \\ \vdots \\ Z_{pq}^{f} \end{pmatrix} \tag{A9}$$

In particular, we have

$$\begin{aligned} Z_{00}^{g} &= \lambda^2 Z_{00}^{f}, \\ \theta_g &= \arg(Z_{1,1}^{g}) = \theta_f - \beta. \end{aligned} \tag{A10}$$

Substitution of Eqs. (A9) and (A10) into Eq. (A8) yields

$$\begin{pmatrix} I^g_{q,q} \\ I^g_{q+2,q} \\ \vdots \\ I^g_{q+2m,q} \end{pmatrix} = e^{-jq\theta_f} e^{jq\beta} diag\left(1,2,\cdots,p+1\right) C_p diag\left(Z_{00}^{f\,-2/2}, Z_{00}^{f\,-3/2}, \cdots, Z_{00}^{f\,-(p+2)/2}\right)$$

$$\times diag\left(\lambda^{-2}, \lambda^{-3}, \cdots, \lambda^{-(p+2)}\right) D_p diag\left(1, \frac{1}{2}, \cdots, \frac{1}{p+1}\right) \begin{pmatrix} Z^g_{0q} \\ Z^g_{1q} \\ \vdots \\ Z^g_{pq} \end{pmatrix}$$

$$= e^{-jq\theta_f} e^{jq\beta} diag\left(1,2,\cdots,p+1\right) C_p diag(Z_{00}^{f\,-2/2}, Z_{00}^{f\,-3/2}, \cdots, Z_{00}^{f\,-(p+2)/2}) \tag{A11}$$

$$\times diag\left(\lambda^{-2}, \lambda^{-3}, \cdots, \lambda^{-(p+2)}\right) D_p diag\left(1, \frac{1}{2}, \cdots, \frac{1}{p+1}\right)$$

$$\times e^{-jq\beta} diag\left(1,2,\cdots,p+1\right) C_p diag\left(\lambda^2, \lambda^3, \cdots, \lambda^{p+2}\right) D_p diag\left(1, \frac{1}{2}, \cdots, \frac{1}{p+1}\right) \begin{pmatrix} Z^f_{0q} \\ Z^f_{1q} \\ \vdots \\ Z^f_{pq} \end{pmatrix}$$

Since

$$\begin{aligned} &diag(1, \frac{1}{2}, \cdots, \frac{1}{p+1}) diag(1,2,\cdots,p+1) = I_p, \\ &D_p C_p = I_p, \\ &diag(\alpha^{-2}, \alpha^{-3}, \cdots, \alpha^{-(p+2)}) diag(\alpha^2, \alpha^3, \cdots, \alpha^{p+2}) = I_p, \end{aligned} \tag{A12}$$

where I_p is the pth order identity matrix, Eq. (A11) becomes

$$\begin{pmatrix} I^g_{0q} \\ I^g_{1q} \\ \vdots \\ I^g_{pq} \end{pmatrix} = e^{-jq\theta_f} diag\left(1,2,\cdots,p+1\right) C_p diag\left(Z_{00}^{f\,-2/2}, Z_{00}^{f\,-3/2}, \cdots, Z_{00}^{f\,-(p+2)/2}\right)$$

$$\times D_p diag\left(1, \frac{1}{2}, \cdots, \frac{1}{p+1}\right) \begin{pmatrix} Z^f_{0q} \\ Z^f_{1q} \\ \vdots \\ Z^f_{pq} \end{pmatrix} = \begin{pmatrix} I^f_{0q} \\ I^f_{1q} \\ \vdots \\ I^f_{pq} \end{pmatrix} \tag{A13}$$

Thus, we have

$$I^g_{pq} = I^f_{pq}. \tag{A14}$$

The proof is now complete.

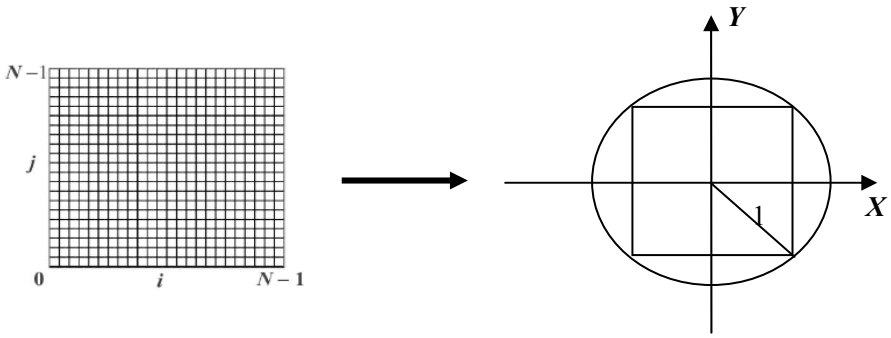

Fig. 1. mapping image inside the unit circle

Fig. 2. The gray image of toy cat

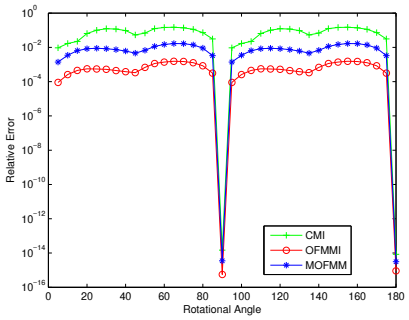

Fig. 3. Performance of the invariants to rotation. Horizontal axis: rotational angle; Vertical axis: relative error between the rotated image and the original image

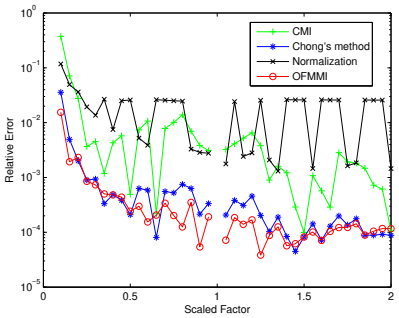

Fig. 4. Performance of the invariants to scale. Horizontal axis: scale factor; Vertical axis:

relative error between the scaled image and the original image

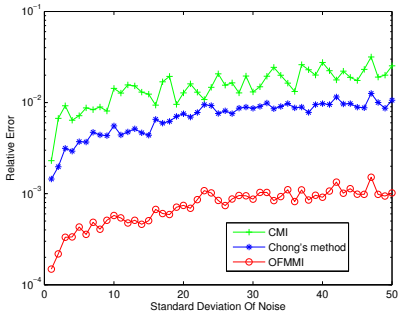

Fig. 5. Performance of the invariants with respect to additive Gaussian zero-mean random noise. Horizontal axis: standard deviation of noise; Vertical axis: relative error between the corrupted image and original image

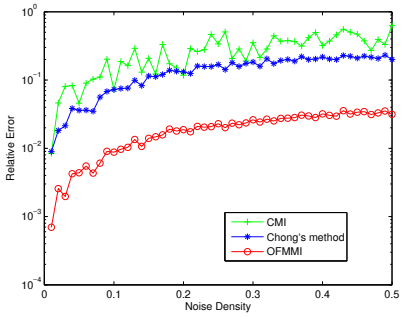

Fig. 6. Performance of the invariants with respect to additive salt-and-pepper noise. Horizontal axis: noise density; Vertical axis: relative error between the corrupted image and original image

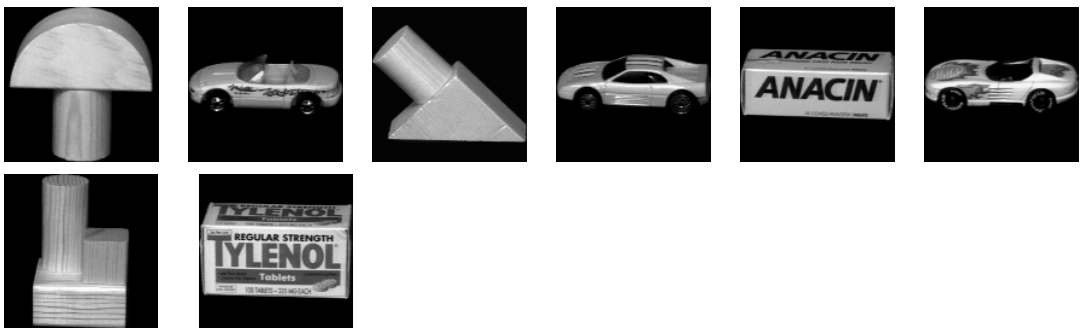

Fig. 7. Original images for invariant object recognition in the experiment

Fig. 8. Original images of alphanumeric characters for invariant character recognition

Fig. 9. Part of the images of the testing set

Table 1 The comparison of CPU elapsed time (s) for the proposed method, complex moment based method and normalization process

	CMI	OFMMI	MOFMM	NMI	Chong's method
Experiment1 (Fig. 3)	21.78	4.97	4.92	-	-
Experiment2 (Fig. 4)	35.53	9.39	-	7.87	10.56
Experiment3 (Fig. 5)	28.42	5.48	-	-	5.5
Experiment4 (Fig. 6)	28.86	5.39	-	-	5.42

Table 2 Classification results of the object images with scale and rotation

	Noise-free	1%	2%	3%	4%
CMI	95.83%	58.75%	50.63%	47.08%	45.63%
Chong's method	98.1%	74.79%	62.08%	54.17%	51.25%
OFMMI	97.50%	85.21%	76.46%	68.96%	58.75%

Table 3 Classification results of the alphanumeric character images with scale and rotation

	Noise-free	1%	2%	3%	4%
CMI	97.40%	58.20%	44.62%	38.54%	32.47%
Chong's method	98%	73.61%	60.24%	50.17%	39.76%
OFMMI	97.40%	80.21%	68.75%	56.60%	44.62%